Artificial Life and Robotics (2022) 27:80–89
https://doi.org/10.1007/s10015-022-00738-x

ORIGINAL ARTICLE

Estimation of blood concentration at different skin depths using a spectroscopic camera

Mengyao Lin[1] · Kaito Iuchi[1] · Kamui Ono[1] · Keiko Ogawa-Ochiai[2] · Norimichi Tsumura[1]

Received: 17 November 2021 / Accepted: 14 January 2022 / Published online: 1 February 2022

Abstract
In this research, we propose a method using a spectroscopic camera to estimate the concentration of blood in different layers of skin tissue. For the demonstration that shows the possibility of application of our method, we conducted a stimulation experiment on 20 subjects involving hot or carbonated baths to promote blood circulation, and estimated the blood concentration before and after stimulation. The results indicate the possibility of estimating blood concentration by proposed method based on spectroscopic images.

Keywords Skin chromophore · Blood · Hemoglobin · Monte Carlo simulation · Spectral reflectance

1 Introduction

Skin is an important source of visual information reflecting conditions of health, beauty, and age. For example, the presence of many age spots on the face may give the impression of old age, and dark circles under the eyes may give the impression of accumulated fatigue. In the beauty industry, many methods and skin care products have been proposed to alleviate or reduce such symptoms [1–3], the cause of which is thought to be chromophores in the skin. The skin has a complicated multi-layered structure (Fig. 1a) over which chromophores may be distributed [4]. For example, age spots are said to be caused by melanin within the skin, and dark circles are said to be caused by melanin and blood [5]. In addition, dark circles are also divided into pigmented dark circles caused by melanin and vascular dark circles caused by poor blood circulation. Different types of dark circles have different treatment methods [6]. If the concentration of melanin and hemoglobin can be accurately measured, appropriate treatment can be taken according to the concentration of chromophores. Melanin, oxy-hemoglobin, and deoxy-hemoglobin exhibit unique light absorption characteristics in the visible wavelength range, and different concentrations of each chromophore change the diffuse reflectance of skin tissue. This means that analysis using diffuse reflectance spectroscopy can provide us with information about the concentrations of melanin and hemoglobin.

Many diffuse reflectance spectroscopy-based methods have been proposed to measure the hemoglobin concentration of the skin. Nishitate et al. [8, 9] proposed a method for estimating tissue oxygen saturation and melanin and blood concentrations in human skin using the Wiener estimation method (WEM) to reconstruct spectral reflectance images from a single snapshot RGB image. Hirose et al. [10] created multiple combinations of chromophores' concentrations and input them into a Monte Carlo Multi-Layered (MCML) algorithm to obtain the spectral reflectance of each combination. A non-linear estimation of chromophores' concentration was performed by creating a relational expression between the chromophores' concentration and reflectance of the skin. Furthermore, a machine that measures the blood volume and blood flow through laser light irradiation of the skin and analysis of the phase differences of the electric fields caused by the movement of red blood cells has been commercialized (OZ-3, Omega Wave Co., Ltd., Tokyo, Japan) [11]. However, this laser-based method can only obtain the average blood volume in the depth direction, and the MCML-based method assumes that the skin structure has only two layers, whereas in reality skin has a multi-layered structure. The measurement of multilayer blood is very important, because skin vessels are generally considered to have two

Mengyao Lin and Kaito Iuchi are equally contributed in this paper.

✉ Kaito Iuchi
k.iuchi@chiba-u.jp

[1] Chiba University, Chiba, Japan

[2] Hiroshima University Hospital, Hiroshima, Japan

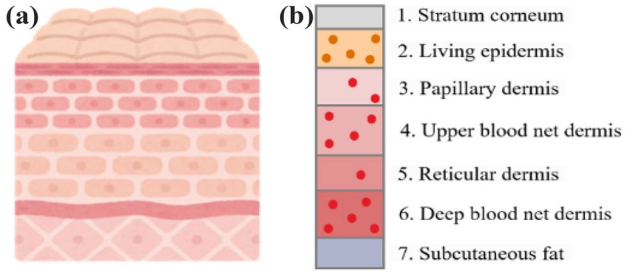

Fig. 1 **a** Cross-sectional image of the skin, **b** seven-layered skin model [4, 7]

major roles. One is in regard to heat transportation for regulating body temperature, which mainly involves blood flow in vessels in the deeper layer, while the other is related to material exchange, such as the supply of nutrients and oxygen, and removal of carbon dioxide, in which capillaries in the surface layer are primarily involved. The difference in these effects is considered to be closely linked with skin condition [12].

In response to this problem, E. Zherebtsov et al. [13] and V. Dremin, et al. [14] proposed a 7-layer skin model. In addition, practice an ANN-based approach to hyperspectral imaging for quantitative diagnostics and characterization of human skin, including 2D mapping of skin chromophores (hemoglobin, melanin, etc.), mapping of blood oxygenation kinetics and evaluation of skin perfusion. In addition, V. Dremin, et al. reported the first clinical application of the system. However, this method requires a lot of data and time when training the data set. Moreover, A. Doronin, et al. [15] proposed a computational tool applied for human finger transmittance spectra simulation and assessment of calibration curve for near infrared transmitted pulse oximetry. However, this method can only measure oxygen saturation and only be applied to fingers. V. Dremin et al. [16] utilized a unified Monte Carlo computational tool, and explore the variations in diagnostic volume due to heart pulse wave for typical transmitted and back-scattered probing configurations used at the pulse oximetry and PPG measurements in a human finger. However, this method can only be applied to fingers, which is limited.

Therefore, in this study, we used a seven-layer model of skin to propose a method for estimating melanin and blood concentrations in skin layers at different depths. First, we used the method of Hirose et al. [10] to perform a Monte Carlo simulation of light transport in multi-layered tissue [17] and derived the function from skin chromophores to absorbance describing the relationship between skin reflectance and chromophores' concentration. Next, we verified the accuracy of the function from skin chromophores to absorbance by estimating values for a numerical phantom in which the chromophores' concentrations had been set in each layer. Then, to demonstrate the possibility of application of our method, we conducted a stimulation experiment with 20 subjects, estimating their blood concentrations before and after stimulation using a warm bath and a carbonated bath.

This paper is an extension of the research presented in 27th Color and Imaging Conference [18]. In this paper, a larger number of subjects was used and a more detailed analysis was done based on the experimental data, considering the insufficiency of demonstration in the previous research [18]. Iuchi et al. have engaged a progressive approach into the method [18] to improve the estimation accuracy [19]. However, the method is demonstrated only with simulation but with actual measurement, while the base method [18] is demonstrated with not enough condition: one subject and one experiment. Therefore, there is a necessity of the detail demonstration of the base method [18], which is a main contribution in this paper.

2 Method

In this Chapter, we describe the proposed method to estimate melanin concentration, blood concentration in skin tissue. The proposed method is based on a regression so that it needs to construct a dataset. To construct a dataset, we obtain various sets of components concentration in skin tissue and corresponding spectral reflectance based on Monte Carlo simulation of light transport in multi-layered tissue (MCML) proposed by Wang et al. [10].

In the first subsection of this section, we describe a creation of a function from skin chromophore concentration into absorbances of skin based on a dataset created with MCML. In the second subsection of this section, we describe a method to estimate skin chromophore concentration and shading from hyperspectral images based on the function from skin chromophore concentration into absorbances of skin. In the third subsection of this section, we describe the optimization of the function from skin chromophore concentration into skin absorbance.

2.1 Analysis of the relationship between absorbance and chromophore concentration

First, the diffuse reflectance data for the skin model were obtained using the MCML method proposed by Jacques et al. [17].

As shown in Fig. 1, we assumed a seven-layered skin model composed of epidermis and dermis [4, 7].

There are several models of skin proposed by some researchers [20, 21]. Compared with the skin models [20,

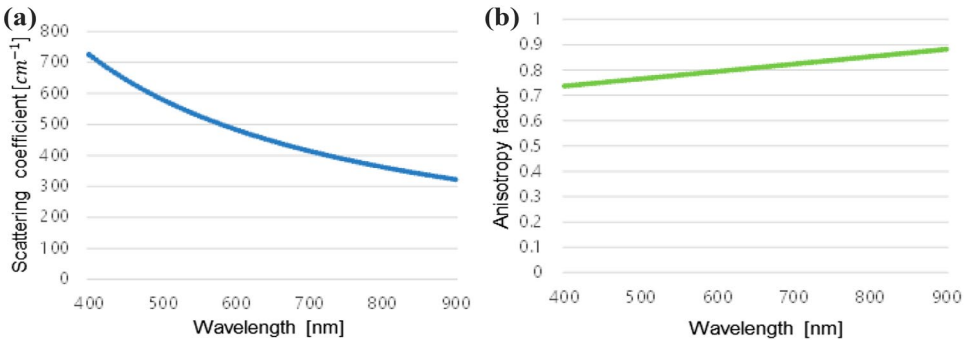

Fig. 2 **a** Scattering coefficient (μ_s) **b** anisotropy factor (g)

21], our skin model is efficient in terms of computational cost on the simulation. MCML requires enormous computational cost depending on the number of parameters of the skin model. In this study, we prioritized the reduction of the parameters used in the skin model. Considering the perspective, we set the chromophores onto the three layers out of the seven layers based on the following knowledge. Melanin is almost localized in the living epidermis [7]. There is a vast vascular plexus in upper blood net dermis and Deep blood net dermis out of seven layers, which has dense blood [7].

The five optical parameters of thickness t, refractive index n, anisotropy factor g, scattering coefficient μ_s, and absorption coefficient μ_a were set for each layer. The parameter n was fixed at 1.4, and μ_s and g were set to the values shown in Fig. 2 [22].

The absorption coefficient μ_a shown in Eq. (1) is calculated from the absorption coefficients of chromophores such as melanin, oxy-hemoglobin, and deoxy-hemoglobin. Considering the computational cost, blood concentration was set for only the 4th and 6th layers, with the other layers being set to 0, because the 4th and 6th layers contain many more blood vessels than the other layers [7]:

$$\begin{aligned}
\mu_{a.epi}(\lambda) &= Mel \times \mu_{a.mel}(\lambda), \\
\mu_{a.der4}(\lambda) &= Ohb_{der4} \times \mu_{a.ohb}(\lambda) + Hb_{der4} \times \mu_{a.hb}(\lambda), \\
\mu_{a.der6}(\lambda) &= Ohb_{der6} \times \mu_{a.ohb}(\lambda) + Hb_{der6} \times \mu_{a.hb}(\lambda),
\end{aligned} \tag{1}$$

where λ is wavelength. The subscripts of epi, $der4$, and $der6$ indicate the epidermis, 4th layer, and 6th layer, respectively. Mel, Ohb, and Hb indicate concentration values of melanin, oxy-hemoglobin, and deoxy-hemoglobin, respectively. The concentration values mean volume concentrations. The absorption coefficients of the chromophores are shown in Fig. 3 [23].

The blood concentration is defined as the sum of oxy-hemoglobin and deoxy-hemoglobin $[Ohb] + [Hb]$. The dataset for the regression is constructed by conducting MCML with multiple combinations of parameters. The dataset consisted of 675 pair data of concentrations of skin chromophores and the corresponding diffuse reflectance of skin

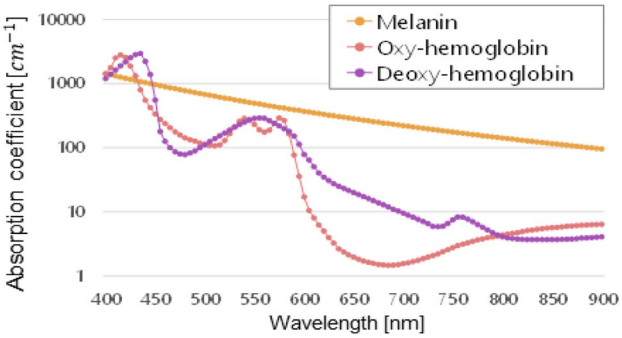

Fig. 3 Absorption coefficients of the chromophores [23]

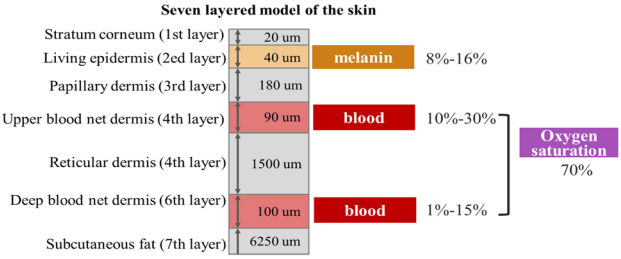

Fig. 4 Set concentrations of the chromophores

$R_{MCML}(\lambda)$. The range of the parameters are represented in Fig. 4. The interval of the parametres of melanin in 4th layer blood in 4th layer, or blood in 6th layer are 2%, 12.5%, and 1%, respectively. Each number of the parameters of melanin in 4th layer, blood in 4th layer, or blood in 6th layer is 5, 9, and 15, respectively.

Next, based on the assumption that surface reflection is removed by the polarizing plate, the reflectance $R_{MCML}(\lambda)$ is converted to absorbance $Abs_{MCML}(\lambda)$ using Eq. (2). We obtained well-fitted curves for 675 absorbance values modeled using the function from skin chromophores to absorbance $Z(Mel, Der_4, Der_6, \lambda)$ for each wavelength, using a least squares function to calculate the sum of the squared

residuals between the absorbance data calculated by MCML and the function from skin chromophores to absorbance the function from skin chromophores to absorbance. This function is shown in Eq. (3). 675 absorbance values are calculated from 675 groups of combinations of melanin and blood concentration percentages. Three types of curved surfaces were modeled. Depending on value of n in Eq. (4), quadratic, cubic, and quartic function are defined. a_k is a coefficient of multiple regression analysis. k is a coefficient number. We have calculated a_k based on conducting multiple regression analysis which is performed by minimizing Eq. (3).

These processes correspond to multiple regression analysis based on second-order, third-order, and fourth-order polynomial models. The reason for the adoption of the higher ordered multiple regression analysis is that the proposed method considers the scattering and absorption of light with a fitting of absorbance by a simulation based on the optical skin model instead of description with the mean path length of light in Modified Lambert Beer, which is dependent on wavelength [23]. This background brings the non-linear relationship between the objective variable and explanatory variable [23]. We discuss which regression model is most appropriate in Sect. 2.3.

$$Abs_{MCML}(\lambda) = -log\big(R_{MCML}(\lambda)\big), \tag{2}$$

$$RSS_{func} = \sum_{i=1}^{675} \big[Abs_{MCML}(i,\lambda) - Z\big(Mel, Der_4, Der_6, \lambda\big)\big]^2, \tag{3}$$

$$Z_n\big(Mel, Der_4, Der_6, \lambda\big) = \sum_{a=0}^{n}\sum_{b=0}^{n}\sum_{c=0}^{n} a_k \times Mel^a \times Der_4^b \times Der_6^c, \tag{4}$$

where RSS_{func} is the squared residual between Abs_{MCML} and Z. $Abs_{MCML}(i,\lambda)$ is the i-th absorbance value by MCML and i indicates the index of the combination of chromophore concentrations.

2.2 Estimation of chromophore concentrations and shading from hyperspectral images

Hirose et al. [10] proposed a method to extract the five components melanin, oxy-hemoglobin, deoxy-hemoglobin, shading, and surface reflection from five-band images of the skin using the cubic function $Z(\lambda)$ represented by Eq. (3). Shading is an element that caused by physical conditions. Physical conditions refer to the physical shape of the object to be photographed and the non-uniformity of lighting. However, to improve the estimation accuracy of the components, we assumed that surface reflection is removed by the polarizing plate. Therefore, the relationship between the diffuse reflection $R(\lambda)$ and absorbance $A(\lambda)$ can be represented as

$$A(\lambda) = -log(R(\lambda)). \tag{5}$$

In the modified Lambert–Beer law, absorbance $A(\lambda)$ can be calculated from the function from skin chromophores to absorbance $Z(\lambda)$ and shading k, as shown in Eq. (6). Shading is added as a constant bias to the absorbance regardless of the wavelength when the spectral characteristics of the illumination are constant regardless of the wavelength or normalized [24]:

$$A(\lambda) = Z(\lambda) + k. \tag{6}$$

The diffuse reflection $R(\lambda)$ is calculated using the following equation based on Eqs. (5) and (6):

$$R(\lambda) = exp(-(Z(\lambda)) + k). \tag{7}$$

In the method, the chromophore concentrations and shading are determined by minimizing the residual sum of squares RSS_{est} as follows:

$$RSS_{est} = \sum_{\lambda} \big[R_{MCML}(\lambda) - (exp(-(Z(\lambda) + k)))\big]. \tag{8}$$

We have utilized the active-set method to minimize Eq. (8) to estimate chromophores' concentrations, which are melanin concentration, blood concentration in 4th layer, and blood concentration in 6th layer (Fig. 5).

2.3 Selection of the optimal function from skin chromophores to absorbance

To select the optimal function from skin chromophores to absorbance, Leave One Out Cross validation was performed. The functions are compared which are defined in Sect. 2.1. The dataset consisting of 675 combinations between skin chromophores and reflectances are used which is defined in Sect. 2.1. The skin chromophores mean melanin concentration, blood concentration in 4th layer, and blood concentration in 6th layer. To assume the condition including an effect

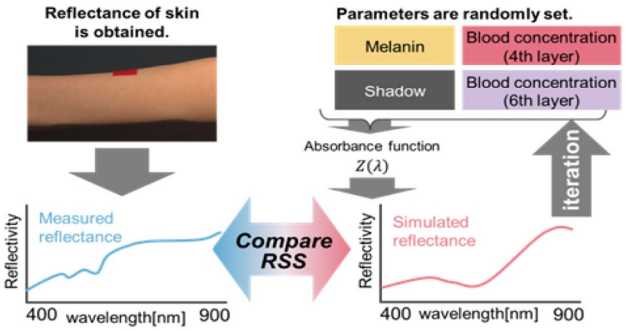

Fig. 5 Outline of the estimation method

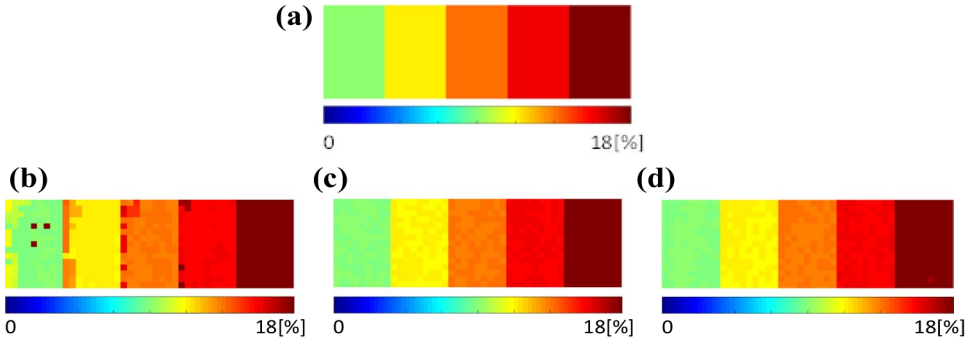

Fig. 6 Maps of estimated melanin (2nd layer of skin model) values: **a** ground truth, **b** by quadratic function, **c** by cubic function, and **d** by quartic function

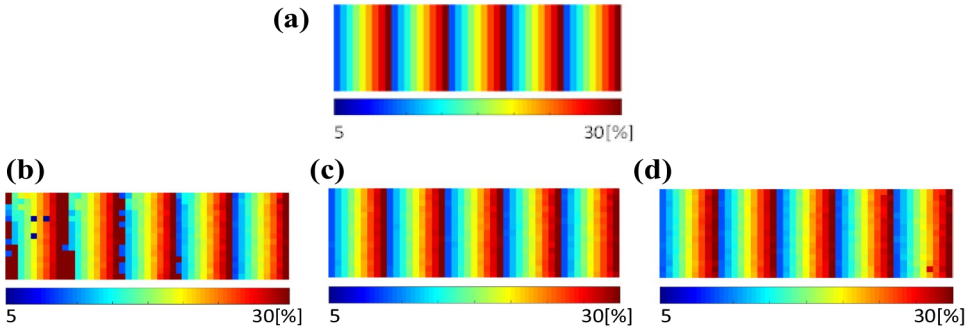

Fig. 7 Maps of estimated 4th-layer blood concentration (4th layer of skin model) values: **a** ground truth, **b** by quadratic function, **c** by cubic function, and **d** by quartic function

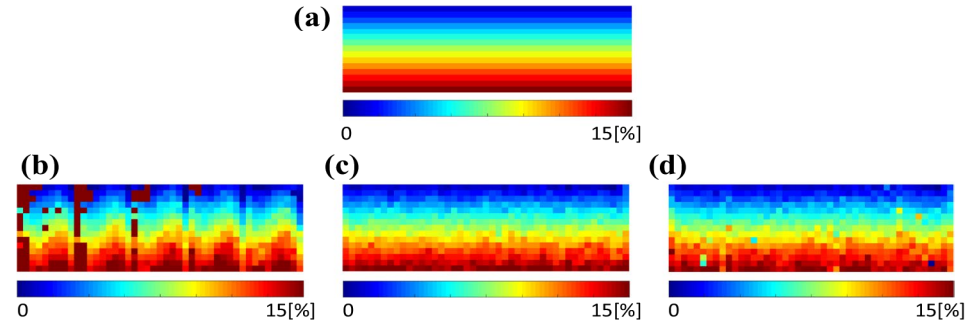

Fig. 8 Maps of estimated 6th-layer blood concentration (6th layer of skin model) values: **a** correct values, **b** by quadratic function, **c** by cubic function, and **d** by quartic function

of shading, the reflectance is added shading by Eq. (9). Here, k indicates shading. In this study, we set k as a constant value of 0.2. As wavelengths, 51 wavelengths sampled at 10 [nm] intervals between 400 and 900 [nm]:

$$R_{MCML,Shading}(\lambda) = R_{MCML}(\lambda) \times \exp(-k). \tag{9}$$

The result of the validation is shown in Figs. 6, 7, and 8 visualized by maps of the ground truths and estimated values colored as a heat map. The combinations of 675 is distributed on a two-dimensional image with 15 pixels vertically and 45 pixels horizontally so as not to include duplication. Figure 6 is a melanin map. Figure 7 is a map of the blood concentration in the 4th layer. Figure 8 is a map of the blood concentration in the 6th layer. Table 1 shows the average relative error of each chromophores' concentration for each type of the function from skin chromophores to absorbance. The relative error is defined by the following equation:

Table 1 Mean relative error when using the three function types

	Melanin	4th-layer blood	6th-layer blood	Shading
Quadratic	0.029	0.20	1.4	0.080
Cubic	0.0012	0.0071	0.075	0.0041
Quartic	0.0021	0.010	0.098	0.0063

$$\text{Relative error} = \left| \frac{\text{Ground truth} - \text{Estimated value}}{\text{Ground truth}} \right| \quad (10)$$

When the quadratic function was used, the estimation accuracy was poor. The cubic function showed better estimation accuracy than the quartic function, and was, therefore, considered the most suitable for estimating chromophore concentrations.

This result has two implications: first, it clarifies the optimal order of the regression model. Second, the estimation accuracy is adequate for data which is not teaching the regressed model, since it is based on Leave One Out, which calculates the estimation accuracy for data which is not on model. The results confirm that the estimation with the regression model has a sufficiently small error for the unknown data. Therefore, the validity of the regression model was considered adequate within the dataset. Our study is an extension of the method proposed by Kobayashi et al. to obtain the relationship between skin chromophores and skin absorbance and the method proposed by Akaho et al. to estimate skin chromophores from skin spectral reflectance to a seven-layered skin model. The method of Akaho et al. estimates the skin chromophores from the skin spectral reflectance based on the two-layer skin model. In their estimation method, the relationship between skin chromophores and skin absorbance of the two-layered skin model is obtained based on the method of Kobayashi et al. This extension has two concerns. First, a contribution of deep layer to skin absorbance could be too small to estimate chromophores. There is a report that the main part of detected skin reflectance becomes localized in the topical upper skin layers including papillary dermis and upper blood net dermis [7]. Second, a contribution of each layer to skin absorbance could be too similar to estimate chromophores. In the two-layered skin model, the components to be estimated have different the absorption coefficient. On the other hand, in the seven-layered skin model, the part of the components to be estimated has the same absorption coefficient: the blood concentration in upper blood net dermis and in deep blood net dermis. This result suggests that the extension of the methods to a seven-layer skin model is achieved without the above concerns exposed. However, the discussed validity of the model is within the simulation so that we have conducted the experiment based on the actual measurement in Chapter 3 and 4.

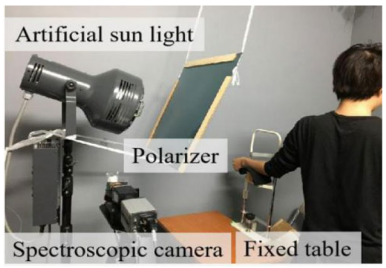

Fig. 9 Experimental environment

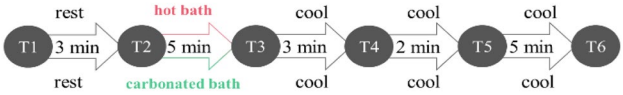

Fig. 10 Experimental protocol

3 Experiment using hot baths and carbonated baths

Figure 9 shows the experimental environment. The measurement setup included an ImSpector spectroscopic camera (JFE Techno Research Corporation, Tokyo, Japan). This camera is a line scan type spectroscopic camera, and the spectroscopic image is acquired by rotating a mirror placed on the turntable. Wavelengths from 400 to 1000 nm can be photographed at a wavelength resolution of 2.8 nm. A SELIC SOLAX500W artificial sunlight light source was used (SERIC, Tokyo, Japan). Polarization filters were placed in front of both the light source and the camera to minimize specular reflection.

Seven female and 13 male volunteers (age: 22.3 ± 0.98 years, body mass: 55.4 ± 5.96 kg, height: 166 ± 6.94 cm) participated in this study. All subjects were physically and mentally healthy at the time of the experiment. The subjects were fully informed of the procedures to be used and the purpose of the study.

The experimental protocol is shown in Fig. 10. Before the experiment, the subjects were asked to sit comfortably in a chair to acclimatize to room temperature (23 ℃) for 5 min. Initially, the subject maintained a comfortable standing position and rested for 3 min. We have applied two types of stimuli, a hot bath and a carbonated bath, to the left forearm and right forearm, respectively. The state of heating is shown in Fig. 11. The size of the bath can fit right into the forearm. We put commercially available bathing agents into the water to generate carbon dioxide. The name of bathing agent is Babu Noukoutannsannyoku SrK1 (Kao Corporation, Tokyo, Japan). The ingredients

Fig. 11 The way to heat a forearm of subject

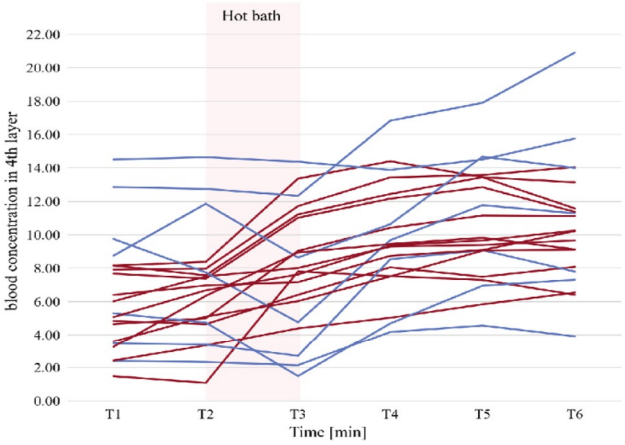

Fig. 12 Changes in the average concentration of blood in the 4th layer following application of a hot bath

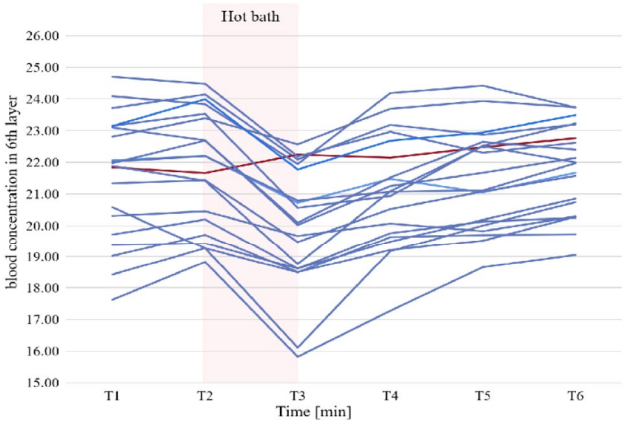

Fig. 13 Changes in the average concentration of blood in the 6th layer following application of a hot bath

Table 2 The ingredients of the bathing agent of Babu Noukoutannsannyoku SrK1 (Kao Corporation, Tokyo, Japan)

Ingredients
Sodium hydrogen carbonate
Sodium carbonate
Calcium carbonate
Fumaric acid
PEG6000
Reduced starch syrup
Isostearic acid
Isostearyl
Trehalose
Sorbeth-60 tetraoleate
Magnesium oxide
Decanoyl/octanoyl-glycerides
Isopropyl palmitate
Glucose
Polyoxyethylene stearyl ether
Glycine
Polyoxyethylene cetyl ether
Polyoxyethylene tridecyl ether sodium acetate
Sucrose fatty acid ester
Oleic acid
Stearic acid
Behenic acid
Sodium hydroxide
Fragrance
Yellow No. 4
Red No. 106

of the bathing agent is shown in Table 2. In addition, an electric thermostat and a water temperature meter were used to control the water temperature so that the initial temperature of hot bath and carbonated bath is between 41 ℃ and 43 ℃. The electric thermostat is NHS-1000S (Shinko Electric Industries Co., Ltd., Nagano, Japan).

Since it is assumed that the temperature does not change during the experiment, a plastic bag was covered on the bath to prevent temperature loss while heating the forearm. After 5 min of the bath, the subject remained relaxed in the same position for 10 min.

4 Results and discussion

Figures 12 and 13, and 14 and 15 show the changes in the average blood concentration with hot baths and carbonated baths, respectively. After carbonated bath and hot bath, the line of blood concentration increasing is marked as red, and the line of blood concentration decreasing is marked as red.

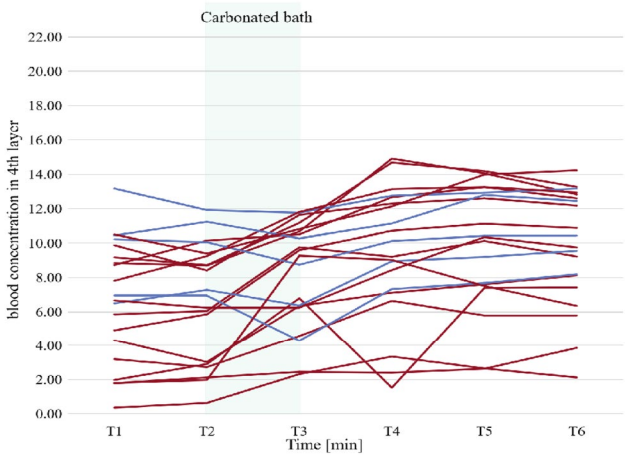

Fig. 14 Changes in the average concentration of blood in the 4th layer following application of a carbonated bath

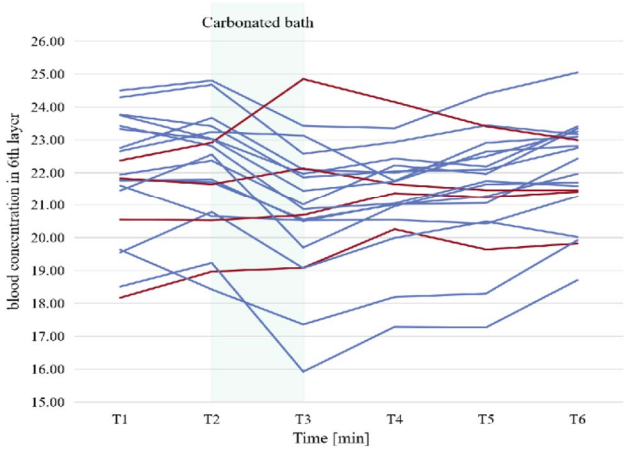

Fig. 15 Changes in the average concentration of blood in the 6th layer following application of a carbonated bath

First, as Figs. 12, 13, 14, and 15 show, there were three different patterns of blood concentration changes following application of a bath (times T2 to T3 in Figs. 12, 13, 14, and 15). The first pattern was a blood concentration increase in both the 4th and 6th layers. The second pattern was a blood concentration increase in the 4th layer but a decrease in the 6th layer. The third pattern was a blood concentration decrease in both the 4th and 6th layers.

To observe the blood changes before and after stimulation more directly, box diagrams were made and paired data was marked shown in Figs. 16 and 17. The red line indicates that the blood concentration increases after stimulation, and the green line indicates that the blood concentration decreases after being stimulated.

As Figs. 16 and 17 show, after hot bath, 13 subjects showed an increase in blood concentration of 4th layer, 1 subject showed an increase in blood concentration of 6th layer. However, after carbonated bath, 15 subjects showed an increase in blood concentration of 4th layer and 4 subjects showed an increase in blood concentration of 6th layer. We performed the Paired sample *T*-test on the data in Figs. 16 and 17, and found that before and after the hot water bath, the P value of the 4th-layer blood was 0.068, and the p value of the 6th-layer blood was 0.023. Before and after the carbonated bath, P value of the 4th-layer blood was 0.006, and the p value of the 6th-layer blood was 0.147. We consider that it is statistically significant when $p < 0.05$. Therefore, it can be considered that the carbonated bath will increase the 4th-layer blood concentration. As mentioned in previous studies [25, 26], the instantaneous blood flow in the skin (right forearm) during CO_2 bathing was significantly increased ($p < 0.05$) compared with freshwater bathing. This conclusion is consistent with the 4th-layer blood concentration in experimental results, and this result indicates the possibility of measuring 4th blood concentration based on our method.

In addition, it can be seen from the results that in hot bath, the p value of the 6th layer's blood concentration change is smaller than 0.05. In combination with (b) in Fig. 17, it can be seen that the blood concentration after stimulation decreases. It is considered that hot bath promotes the expansion of the 4th layer's blood vessels first, while the 6th layer's blood vessels have not received stimulation at the same time, so the blood moves to the 4th layer and the 6th layer's blood concentration decreases.

However, since no previous research has been found on the changes of different layers of blood concentration in the hot bath and carbonated bath, we cannot show the accuracy of the results of the 6th-layer blood concentration. In the future, we will use a blood flow meter (Oxygen to See, LEA Medizintechnik GmbH, Giessen, Germany) which can measure different layers blood flow to test the accuracy of our method.

Each subject's blood concentration changed differently following stimulation. The reasons for this are thought be related to the individual's physical condition, autonomic nervous system, and mood (tension) during the experiment. In future work, we plan to measure the changes in subjects' heart rates to determine the effects of hot baths and carbonated baths on autonomic nerves. Moreover, we will change the values of scattering coefficient and absorption coefficient to observe the effect on reflectivity and results.

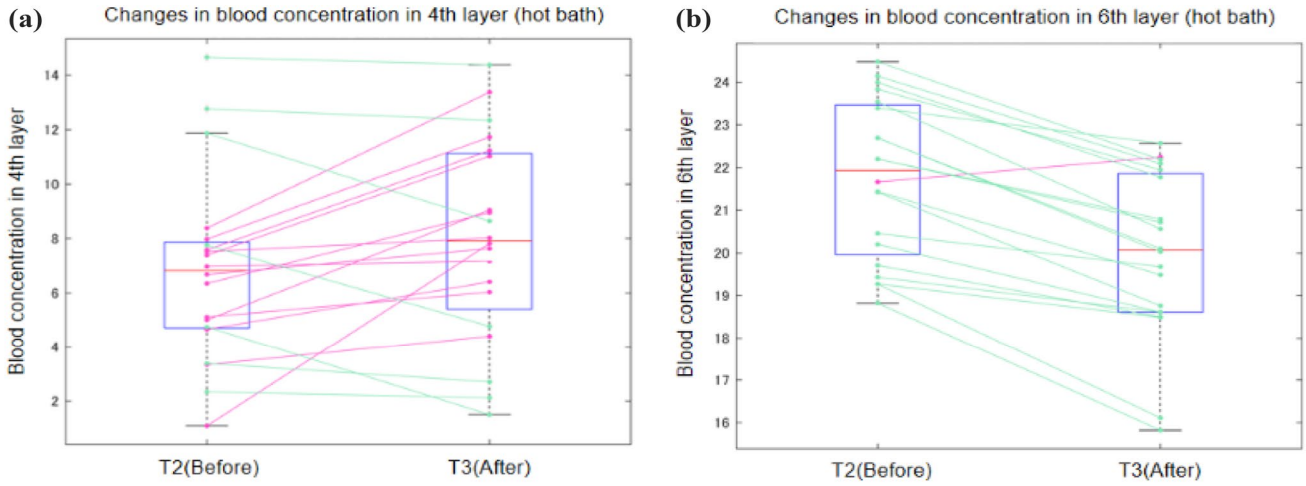

Fig. 16 Changes in blood concentration before and after hot bath: **a** in 4th layer, **b** in 6th layer

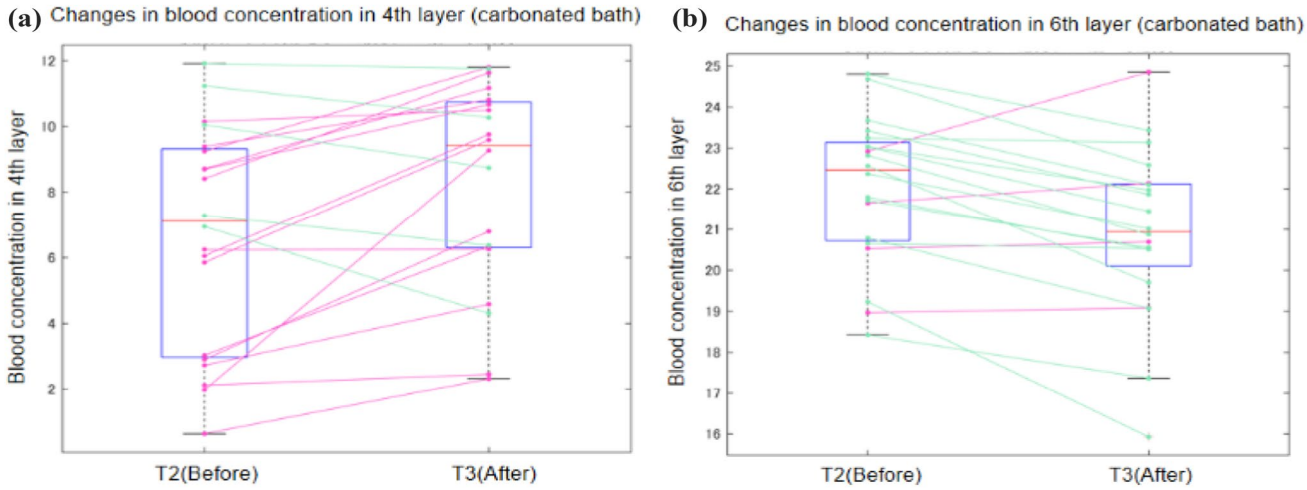

Fig. 17 Changes in blood concentration before and after carbonated bath: **a** in 4th layer, **b** in 6th layer

5 Conclusions

We proposed a skin blood concentration measurement method based on a spectroscopic camera. Our method has a capability to estimate skin chromophore concentrations in skin layers of different depths. For the demonstration that shows the possibility of application of our method, we conducted the experiment in which we estimated the blood concentration of 20 subjects based on the spectroscopic image of the skin. In addition, we observe changes in blood concentration by stimulation experiments. Since these estimated results can be explained by previous experimental conclusion, the results indicate the possibility of blood concentration estimation based on spectroscopic images. In future research, we will change the thickness of the seven-layered model and observe the influence of the thickness on the experimental results. In addition, to reduce the influence of individual differences on the experimental results, the heart rate of the subjects will be measured in the future experiment to determine the changes of personal autonomic nerves.

Acknowledgements We thank Karl Embleton, PhD, from Edanz Group (https://en-author-services.edanzgroup.com/ac) for editing a draft of this manuscript.

Declarations

Conflict of interest The authors declare no conflicts of interest.

References

1. Ohshima H, Mizukoshi K, Oyobikawa M et al (2009) Effects of vitamin C on dark circles of the lower eyelids: quantitative evaluation using image analysis and echogram. Skin Res Technol 15:214–217
2. Mitsuishi T, Shimoda T, Mitsui Y et al (2004) The effects of topical application of phytonadione, retinol and vitamins C and E on infraorbital dark circles and wrinkles of the lower eyelids. J Cosmet Dermatol 3:73–75
3. Serra M et al (2018) Brightening and improvement of facial skin quality in healthy female subjects with moderate hyperpigmentation or dark spots and moderate facial aging. J Drugs Dermatol 17:1310–1315
4. BASF Personal Care (2021) https://www.carecreations.basf.com/news-media/photos-and-illustrations/photosandillustrations-detail/2006/1/14/the-skin-s-blood-vessel-system. Accessed 1 Feb 2022
5. Freitag FM, Cestari TF (2007) What causes dark circles under the eyes. J Cosmet Dermatol 6:211–215
6. Park SR, Kim HJ, Park HK (2016) Classification by causes of dark circles and appropriate evaluation method of dark circles. Skin Res Technol 22(3):276–283
7. Meglinski IV, Matcher SJ (2003) Computer simulation of the skin reflectance spectra. Comput Methods Programs Biomed 70:179–186
8. Nishidate I, Maeda T, Niizeki K et al (2013) Estimation of melanin and hemoglobin using spectral reflectance images reconstructed from a digital RGB image by the Wiener estimation method. Sensors 13:7902–7915
9. Shimada M et al (2000) Explanation of human skin color by multiple linear regression analysis based on the Modified Lambert-Beer law. Opt Rev 7:348–352
10. Hirose M, Tsumura N (2015) Nonlinear estimation of chromophore concentrations, shading and surface reflectance from five band images. In: Proceedings of Color and Imaging Conference, Darmstadt, Germany, pp 161–166.
11. Omega Wave Co. Ltd. (2021) http://www.omegawave.co.jp/. Accessed 1 Feb 2022
12. Oharazawa A, Ogino M, Sugahara M (2020) Skin capillary extraction technique based on independent component analysis and Frangi filter using videomicroscopy. Skin Res Technol 26(5):664–670
13. Zherebtsov E, Dremin V et al (2019) Hyperspectral imaging of human skin aided by artificial neural networks. Biomed Opt Express 10(7):3545–3559
14. Dremin V et al (2021) Skin complications of diabetes mellitus revealed by polarized hyperspectral imaging and machine learning. IEEE Trans Med Imaging 40:1207–1216
15. Doronin A, Fine I, Meglinski I (2011) Assessment of the calibration curve for transmittance pulse-oximetry. Laser Phys 21(11):1972–1977
16. Dremin V et al (2019) Influence of blood pulsation on diagnostic volume in pulse oximetry and photoplethysmography measurements. Appl Opt 58(34):9398–9405
17. Wang L, Jacques SL (1992) Monte carlo modeling of light transport in multi-layered tissues in standard C. University of Texas M. D. Anderson Cancer Center, Houston
18. Iuchi K, Akaho R, Igarachi T, Ojima N, Tsumura N (2019) Estimation of blood concentration in skin layers with different depths. Color Imaging Conf 2019(1):290–294
19. Iuchi K, Nomura I, Igarashi T, Ojima N, Tsumura N (2020) Estimation of melanin concentration, blood concentration, and oxygen saturation in skin tissue layers with different depths unaffected by shading. Imaging Manip Anal Biomol Cell Tissues XVIII 11243:112430I
20. Hernandez-Quintanar L, Fabila-Bustos DA, Hernandez-Chavez M, Valor A, Rosa JM, Stolik S (2020) Fiber-optic pulseoximeter for local oxygen saturation determination using a Monte Carlo multi-layer model for calibration. Comput Methods Programs Biomed 187:1055237
21. Takaaki M, Arakawa N, Takahashi M, Aizu Y (2010) Monte Carlo simulation of spectral reflectance using a multilayered skin tissue model. Opt Rev 17(3):223–229
22. Tsumura N, Kawabuchi M et al (2000) Mapping pigmentation in human skin from multi-channel visible spectrum image by inverse optical scattering. Technique. J Imaging Sci Technol 45:444–450
23. Oregon Medical Laser Center, Optical Properties Spectra (2021). http://omlc.org/spectra/
24. Akaho R, Hirose M, Tsumura N (2018) Evaluation of the robustness of estimating five components from a skin spectral image. Opt Rev 25(2):181–189
25. Nishimura N, Sugenoya J, Matsumoto T et al (2002) Effects of repeated carbon dioxide-rich water bathing on core temperature, cutaneous blood flow and thermal sensation. Eur J Appl Physiol 87:337–342
26. Xu FH et al (2009) Immediate physiological changes induced by a carbon dioxide footbath on circulatory and autonomic nervous systems in healthy males. J Jpn Soc Balneol Climatol Phys Med 72:216–228